Physics Reports 1202 (2027) 1–16

Contents lists available at ScienceDirect

Physics Reports

journal homepage: www.elsevier.com/locate/physrep

Review article

Orbital homology of p and t_{2g} orbitals in models and materials

Gang v. Chen [a,b,c,d,*], Congjun Wu [e,f,g,h]

[a] International Center for Quantum Materials, School of Physics, Peking University, Beijing 100871, China
[b] Tsung-Dao Lee Institute, Shanghai Jiao Tong University, Shanghai 201210, China
[c] Collaborative Innovation Center of Quantum Matter, 100871, Beijing, China
[d] Beijing Key Laboratory of Quantum Devices, Peking University, Beijing 100871, China
[e] New Cornerstone Science Laboratory, Department of Physics, School of Science, Westlake University, Hangzhou 310024, Zhejiang, China
[f] Institute of Natural Sciences, Westlake Institute for Advanced Study, Hangzhou 310024, Zhejiang, China
[g] Institute for Theoretical Sciences, Westlake University, Hangzhou 310024, Zhejiang, China
[h] Key Laboratory for Quantum Materials of Zhejiang Province, School of Science, Westlake University, Hangzhou 310024, Zhejiang, China

ARTICLE INFO

Article history:
Received 18 March 2026
Received in revised form 31 July 2026
Accepted 7 August 2026

Editor: Naoto Nagaosa

Keywords:
Orbital homology
Luttinger model
Band topology
Itinerant ferromagnetism
Unconventional superconductivity
Transition metal compounds
Two-dimensional oxide heterostructures
Iron-based superconductors
p-orbital ultracold gases

ABSTRACT

The nominal divide between p- and d-electron systems often obscures a deep underlying unity in condensed matter physics. This review elucidates the orbital homology between the p and t_{2g} orbital manifolds, establishing the correspondence that extends from minimal model Hamiltonians to the complex behaviors of real quantum materials. We demonstrate that despite their distinct atomic origins, these orbitals host nearly identical hopping physics and spin–orbit coupling, formalized through an effective $l = 1$ angular momentum algebra for the t_{2g} case. This equivalence allows one to transpose physical intuition and theoretical models developed for p-orbital systems directly onto the more complex t_{2g} materials, and vice versa. We showcase how this paradigm provides a unified understanding of emergent phenomena, including non-trivial band topology, itinerant ferromagnetism, and unconventional superconductivity, across a wide range of platforms, from transition metal compounds, two-dimensional oxide heterostructures, and iron-based superconductors, to p-orbital ultracold gases. Ultimately, this p-t_{2g} homology serves not only as a tool for interpretation but also as a robust design principle for engineering novel quantum states.

© 2026 Elsevier B.V. All rights are reserved, including those for text and data mining, AI training, and similar technologies.

Contents

* Corresponding author at: International Center for Quantum Materials, School of Physics, Peking University, Beijing 100871, China.
E-mail addresses: chenxray@pku.edu.cn (G.v. Chen), wucongjun@westlake.edu.cn (C. Wu).

https://doi.org/10.1016/j.physrep.2026.08.003
0370-1573/© 2026 Elsevier B.V. All rights are reserved, including those for text and data mining, AI training, and similar technologies.

1. Introduction

In a fundamental sense, condensed matter physics and quantum materials are concerned with the microscopic constituents of physical degrees of freedom, their intrinsic properties, and the interactions among them. Understanding the microscopic nature of these physical degrees of freedom is therefore of paramount importance, and electron orbitals constitute one of the essential degrees of freedom for electrons [1,2]. Traditionally, the physics of p-electron systems (originating from $l = 1$ orbitals), and d-electron systems ($l = 2$) have been treated in largely separate domains. The former are central to the chemistry and physics of sp-bonded materials like semiconductors, graphene, and molecular solids, while the latter dominate the rich and complex world of transition metal compounds [3,4], renowned for phenomena such as high-temperature superconductivity, colossal magnetoresistance, and metal–insulator transitions. This conventional separation, however, obscures a profound and powerful underlying unity. An orbital homology exists between the p orbital manifold and the t_{2g} subset of d orbitals, a correspondence that transcends their distinct atomic origins and provides a unified conceptual framework for understanding and designing quantum phenomena across a vast range of materials.

This equivalence is not merely a mathematical curiosity but a physical reality rooted in the fundamental principles of group theory. In an octahedral crystal field (see Fig. 1), the five-fold degeneracy of the atomic d orbitals is lifted, splitting them into a high-energy e_g doublet ($d_{x^2-y^2}$, d_{z^2}) and a low-energy t_{2g} triplet (d_{xy}, d_{xz}, d_{yz}). The transformational properties of these t_{2g} orbitals under the symmetry operations of the octahedral group (O_h) are isomorphic to those of the p orbital triplet (p_x, p_y, p_z). This algebraic homology permits a direct mapping:

$$d_{yz} \leftrightarrow -|p_x\rangle, \quad d_{xz} \leftrightarrow |p_y\rangle, \quad d_{xy} \leftrightarrow -|p_z\rangle. \tag{1}$$

This mapping establishes that the t_{2g} manifold behaves as an effective orbital angular momentum $L_{\text{eff}} = 1$ system (see Fig. 1). The effective angular momentum formalism for the t_{2g} manifold has a long history, dating back to the early crystal-field theories of Van Vleck [5] and the paramagnetic resonance studies of Pryce [6], and was later systematized in the classic works of Griffith [7] and Abragam and Bleaney [8]. In particular, the isomorphism between the t_{2g} triplet and the p orbitals was recognized long ago and has been fruitfully exploited in the contexts such as magnetic resonance, Jahn-Teller physics, and optical spectroscopy. This foundational insight is the cornerstone of their homology, dictating parallel behaviors in two relevant regimes, *i.e.* electronic hopping and spin–orbit coupling.

The orbital homology manifests most immediately in the kinetic energy of these electrons. The hopping amplitudes between orbitals on adjacent lattice sites are governed by the overlap of their wavefunctions, which is constrained by their symmetry and orientation. For instance, a p_x orbital hops strongly along the x-direction through σ-bonding, but only weakly along y via π-bonding. Similarly, a d_{xz} orbital hops strongly along the x-direction with a strong π-overlap of its xz-lobe but negligibly along y with a weak δ-overlap in 2D (see Fig. 2). This directional anisotropy is a hallmark of both manifolds. Consequently, the tight-binding models constructed for the t_{2g} electrons in two-dimensional lattices are quite analogous to those for the p electrons in the same structure. This may allow researchers to leverage the more intuitive geometry of the p orbitals to construct and solve models for the more complex d-electron systems, translating insights directly from one realm to the other.

The homology becomes much more useful with the inclusion of spin–orbit coupling (SOC), the key ingredient for many topological and/or correlated states. For atomic p electrons, SOC takes the standard form $H_{\text{soc}} = \lambda \mathbf{L} \cdot \mathbf{S}$, where $\mathbf{L}$ is the genuine $l = 1$ angular momentum operator. For the t_{2g} electrons, the physical $l = 2$ angular momentum is projected into the t_{2g} subspace. Remarkably, the resulting operators $\mathbf{L}_{\text{eff}}$ obey the commutation relations of an $l = 1$ algebra (see Fig. 1). This leads to an identical SOC Hamiltonian for the t_{2g} system, $H_{\text{soc}}^{t_{2g}} = -\lambda_{\text{soc}} \mathbf{L}_{\text{eff}} \cdot \mathbf{S}$, except the minus sign. This is a remarkable simplification. It implies that the complex SOC-driven physics in t_{2g} materials, such as the formation of the celebrated $j_{\text{eff}} = 1/2$ ground state in strontium iridates Sr_2IrO_4 [9–12], is directly analogous to the SOC physics in the p-orbital systems, though the former is more correlated. This shared platform enables the prediction and interpretation of topological insulators, Rashba effects, and topological superconductivity in t_{2g} materials based on principles understood and explored in the p-orbital contexts.

The power of this paradigm is its ability to bridge the gap from the abstract models to real materials. We demonstrate this orbital homology across three principal domains. In Section 2, we explore the theoretical foundations and the material realizations of the orbital homology in topological and correlated phases. We begin with the Luttinger semimetal, showing how both p-orbital semiconductors and t_{2g}-based transition metal compounds exhibit identical quadratic band touching physics described by isomorphic Hamiltonians. We further mention how the Kane–Mele model and concepts of fragile

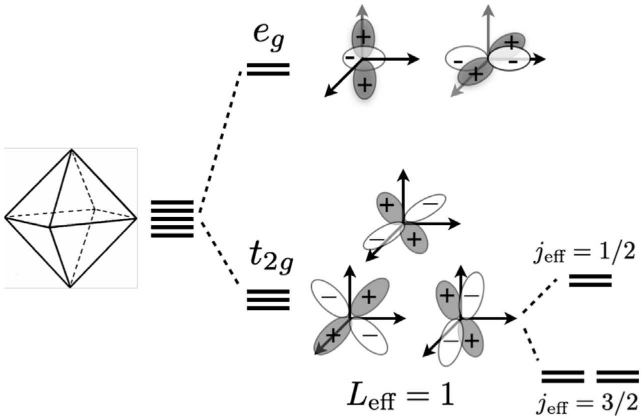

Fig. 1. Schematic energy level diagram of d-electron splitting under an octahedral crystal field, followed by the effects of spin–orbit coupling. The crystal field lifts the degeneracy of the d-orbitals, splitting them into higher-energy e_g and lower-energy t_{2g} levels. With the inclusion of spin–orbit coupling, the t_{2g} manifold further splits into a higher-energy $j_{\text{eff}} = 1/2$ doublet and a lower-energy $j_{\text{eff}} = 3/2$ quartet, corresponding to effective orbital angular momentum $L_{\text{eff}} = 1$.

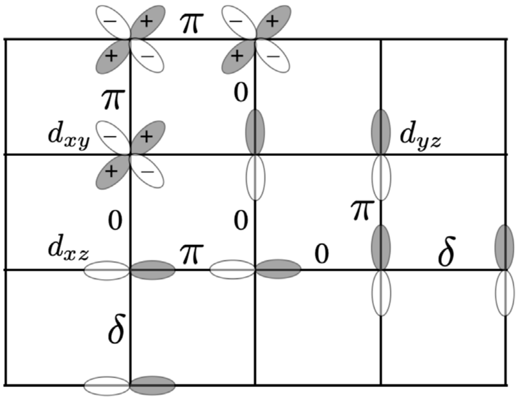

Fig. 2. Orbital-specific hoppings in a square lattice. d_{xz} and d_{yz} orbitals form π-bonds along x and y directions, respectively, while d_{xy} exhibits the π bonding along both x and y directions. The symmetry-demanded 0 hopping and the weak δ hopping are marked as well.

topology find parallel realizations in both orbital systems, establishing a unified framework for understanding topological phase transitions across diverse material platforms including half-Heusler compounds and pyrochlore iridates. Section 3 examines two-dimensional materials and interfaces, where the quantum confinement and symmetry breaking create ideal conditions for observing the functional equivalence. We analyze the oxide heterostructures such as $LaAlO_3/SrTiO_3$ and $LaAlO_3/KTaO_3$, showing how the emergent physics of the t_{2g} orbitals mirrors that of the p-orbital systems in anisotropic hopping, Rashba spin–orbit coupling, and nematic superconductivity. The remarkable parallel between t_{2g}-based oxide interfaces and p-orbital topological insulators like Cu-doped Bi_2Se_3 highlights the universal role of spin–orbit coupling in driving unconventional superconducting states. The extension to iron-based superconductors is further elaborated. Finally, Section 4 investigates the ultracold atoms in optical lattices as pristine quantum simulators for t_{2g} physics. We demonstrate how the p-orbital optical lattices can mimic the essential physics of the t_{2g} electron systems, enabling controlled studies of orbital ordering, magnetic frustration, and itinerant ferromagnetism without solid-state complications. This platform provides crucial insights into multi-orbital correlation effects and serves as an experimental testbed for theoretical predictions. In Section 5, we provide a summary about the current understanding and vision the future application of this p-t_{2g} orbital correspondence.

2. Orbital homology in topological and correlated phases

The orbital homology between the p and t_{2g} orbital systems extends across the landscape of quantum materials, providing a more-or-less unified framework for understanding both topological phases and correlated electron phenomena. This section explores the homology between these orbital manifolds through their theoretical realizations in model Hamiltonians and their material manifestations in topological and correlated phases.

2.1. Theoretical models

The isomorphic orbital algebra shared by the p and t_{2g} manifolds means that minimal models for topological phases can be implemented on both p-orbital and t_{2g}-derived effective lattices with nearly identical outcomes. The Luttinger semimetal represents a fascinating class of quantum materials where the electron bands touch quadratically at discrete points in the Brillouin zone, creating unique electronic properties that bridge the gap between conventional metals and insulators. More significantly, the Luttinger semimetal is recognized as a parent state for numerous topological phases; through various perturbations, it can give rise to topological insulators, Weyl semimetals, Dirac semimetals, and other exotic states. In the modern nomenclature, the Luttinger semimetal is an example of topological crystalline semimetal [13,14]. The physics of these Luttinger semimetallic systems finds remarkably parallel realizations in both p-orbital semiconductors and t_{2g}-based transition metal compounds, revealing the homology between these orbital manifolds.

In the p-orbital semiconductor systems, particularly those with zincblende or diamond crystal structures, the Luttinger Hamiltonian emerges naturally from the coupling between the orbital and spin degrees of freedom. The derivation begins with the p-orbital basis (p_x, p_y, p_z) coupled with the electron spin, forming a six-dimensional Hilbert space. The strong spin–orbit coupling $H_{\rm soc} = \lambda \mathbf{L} \cdot \mathbf{S}$ mixes these states, where $\mathbf{L}$ are the $l = 1$ orbital angular momentum operators. When projected to the total angular momentum $j = 3/2$ subspace, one obtains the celebrated Luttinger Hamiltonian [15],

$$H_L = \frac{\hbar^2}{2m}\Big[\gamma_1 k^2 - 2\gamma_2 \sum_i k_i^2 J_i^2 - 4\gamma_3 \sum_{i<j} k_i k_j \{J_i, J_j\}\Big] \tag{2}$$

where $\mathbf{J}$ represents the 4×4 spin-3/2 matrices satisfying the SU(2) algebra, and the Luttinger parameters γ_1, γ_2, γ_3 characterize the material-specific band structure. Here, $\{J_i, J_j\} = \frac{1}{2}(J_i J_j + J_j J_i)$. The cubic anisotropy term with J_i, J_j reflects the underlying crystal symmetry and leads to the characteristic band warping effects observed in materials like Ge, GaAs, α-Sn, and HgTe [16–18]. A schematic dispersion for Luttinger model is depicted in Fig. 3 for GaAs [19].

Remarkably, an isomorphic mathematical structure emerges in the t_{2g} electron systems despite their different orbital origin. Starting from the t_{2g} manifold (d_{xy}, d_{xz}, d_{yz}) with the strong spin–orbit coupling $H_{\rm soc} = -\lambda_{\rm soc} \mathbf{L}_{\rm eff} \cdot \mathbf{S}$, the effective orbital angular momentum operators $\mathbf{L}_{\rm eff}$ obey the $l = 1$ algebra due to the fundamental homology between the t_{2g} and p orbitals. Through the explicit mapping $d_{yz} \leftrightarrow -|p_x\rangle$, $d_{xz} \leftrightarrow |p_y\rangle$, $d_{xy} \leftrightarrow -|p_z\rangle$ in Section 1, the t_{2g} Hamiltonian transforms into,

$$H_{\rm eff}^{t_{2g}} = \frac{\hbar^2}{2m_{\rm eff}}\Big[\tilde{\gamma}_1 k^2 - 2\tilde{\gamma}_2 \sum_i k_i^2 \tilde{J}_i^2 - 4\tilde{\gamma}_3 \sum_{i<j} \{\tilde{J}_i, \tilde{J}_j\} k_i k_j\Big] \tag{3}$$

where $\tilde{\mathbf{J}}$ represents the effective spin-3/2 operators in the $j_{\rm eff} = 3/2$ subspace, and the renormalized parameters $\tilde{\gamma}_i$ incorporate both the bare electron mass and correlation effects specific to t_{2g} systems.

While the Luttinger model itself only requires a symmetry-protected fourfold degeneracy at the Γ point to describe its essential properties, this symmetry-based requirement overlooks the orbital character and microscopic origins of the underlying degrees of freedom. It is precisely the recognition that this model can be physically realized through both the genuine $j = 3/2$ states of p-orbitals and the effective $j_{\rm eff} = 3/2$ states of the t_{2g} orbitals that underscores the significance of their orbital homology. Beyond the established realization of the Luttinger semimetal through the $j_{\rm eff} = 3/2$ states of t_{2g} orbitals, it has been recently discovered that materials like pyrochlore iridate $Pr_2Ir_2O_7$ can host a Luttinger semimetal phase emerging from $j_{\rm eff} = 1/2$ states (see Fig. 4 and Section 2.2) [20–22]. In this scenario, the band index is partially provided by the pyrochlore's sublattice degree of freedom. This mechanism fundamentally transcends the conventional microscopic requirement of a $j = 3/2$ angular momentum composition for the Luttinger model. Furthermore, leveraging the p-t_{2g} equivalence, we can predict that p-orbital $j = 1/2$ states on an appropriate non-Bravais lattice should similarly give rise to a Luttinger semimetal, generalizing the platform for this physics beyond its original conceptual boundaries.

The significance of this equivalence extends beyond the academic interest, as Luttinger semimetal serve as a versatile parent states for numerous topological phases [17,20,21,23,24]. In both p-orbital and t_{2g} realizations, breaking time-reversal symmetry through magnetic doping or external fields can transform the quadratic band touching into Weyl nodes, creating Weyl semimetals. Similarly, uniaxial strain or chemical pressure can lift the cubic symmetry, leading to Dirac semimetals or topological insulators depending on the perturbation direction and strength. The equivalence and homology ensure that the topological phase diagrams derived for p-orbital Luttinger semimetals directly inform the behavior of their t_{2g} counterparts. Even for the non-topological models and phases, the orbital homology is expected to be quite useful. The spin–orbit-coupled metal has been proposed to understand the parent metallic state and the parity-breaking electronic nematic phase in the pyrochlore material $Cd_2Re_2O_7$ that is based on the spin–orbit coupling of the t_{2g} electrons [25–27]. The actual building-up of the spin–orbit-coupled metallic model with the Landau Fermi-liquid-like approach, however, is quite general, and can be well suited for the p-orbital metals.

Although not as direct as the Luttinger semimetal, the Kane–Mele model [28,29], a cornerstone of topological insulators, provides another compelling demonstration of this equivalence between p and t_{2g} orbitals. Originally conceived for spinful p_z orbitals on a honeycomb lattice with spin–orbit coupling, it predicts the quantum spin Hall effect. Remarkably, the same topological phase can be realized in t_{2g} systems. In materials such as the honeycomb iridate Na_2IrO_3 [30] or engineered

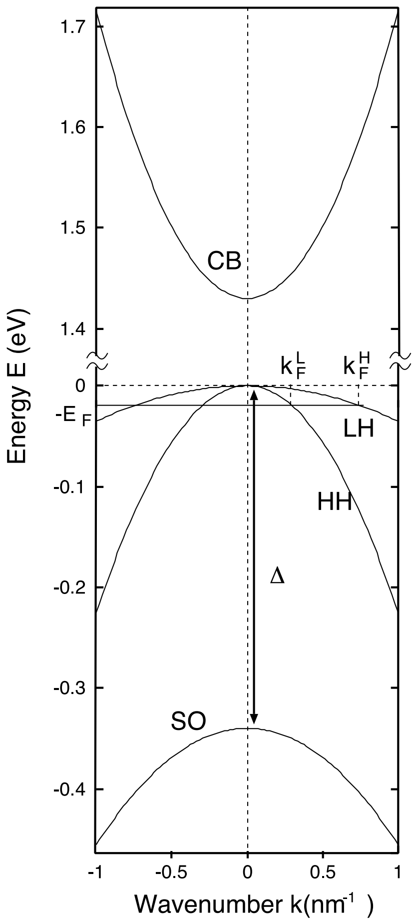

Fig. 3. Schematic picture of the band structure of GaAs near $k = 0$. CB means the conduction band, HH the heavy-hole band, LH the light-hole band, and SO the split-off band, respectively. When the small inversion symmetry breaking is neglected, all of them are doubly degenerate. The splitting Δ at $k = 0$ between the LH,HH and SO bands are due to the spin–orbit coupling.
Source: Figure is adapted from Ref. [19].

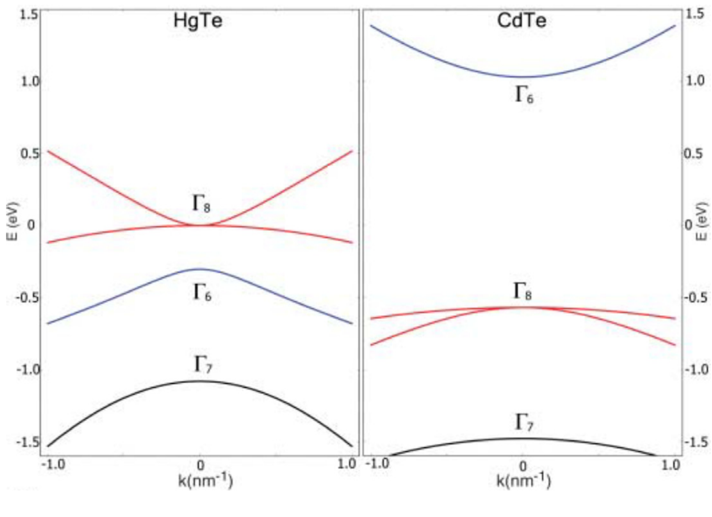

Fig. 4. Comparison of the bulk band structures of CdTe and HgTe at the Γ point. In CdTe, the Γ_6 s-like conduction band lies above the Γ_8 *p*-like valence band. In HgTe, strong spin–orbit coupling inverts this order, placing the Γ_8 (heavy-hole) band above the Γ_6 band. The Luttinger model Hamiltonian, parameterized by γ_1, γ_2, and γ_3, captures the degenerate Γ_8 valence band structure in both semiconductors.
Source: Figure is adapted from Ref. [16].

oxide heterostructures [31–34], the t_{2g} orbitals on a honeycomb lattice, when subjected to strong spin–orbit coupling, were proposed to yield identical topological invariants and protected edge states, though Na_2IrO_3 was more popularly proposed as the Mott insulating Kitaev material due to the spin–orbit entangled $j = 1/2$ [35]. Similarly, concepts of fragile topology characterized by Wilson loop invariants find parallel realizations in both orbital families [36–38]. The nontrivial braiding of Wilson loops in the Brillouin zone, which signals fragile topology, depends on the specific orbital matrix elements and Berry connections. Since these are determined by the symmetry properties and algebra of the orbital basis, the identical transformation properties of p and t_{2g} orbitals guarantee that Wilson loop diagnostics yield equivalent results.

This underlying equivalence between the p-orbital and t_{2g} realizations establishes a powerful paradigm for topological materials design, providing a robust conceptual framework that significantly accelerates the discovery and understanding of novel quantum states. The orbital homology and functional equivalence serve as a powerful design principle whereby theoretical predictions of topological phases in conceptually simpler p-orbital models can be directly translated to the more complex t_{2g} materials, enabling efficient exploration of exotic quantum matter with tailored properties.

2.2. Material realizations across orbital systems

The theoretical homology between the p and t_{2g} orbitals finds exquisite experimental realization across diverse material platforms, spanning from conventional semiconductors to complex correlated oxides. This material diversity illustrates the universal nature of orbital physics in determining the electronic behavior, demonstrating that the essential quantum phenomena are encoded not just in the specific atomic origins but also in the orbital characters.

In the p-orbital realm, half-Heusler compounds like LaBiPt and YPtBi provide exceptional platforms for studying the Luttinger semimetal physics with strong spin–orbit coupling [39]. These materials exhibit the characteristic quadratic band touching predicted by the Luttinger Hamiltonian, serving as excellent testbeds for topological phases. Under appropriate perturbations (such as chemical substitution, hydrostatic pressure, or uniaxial strain), these p-orbital systems can be driven into various topological states including Weyl semimetals and topological insulators. Simultaneously, in the t_{2g} domain, pyrochlore iridates such as $Pr_2Ir_2O_7$ and the related compounds display analogous quadratic band touching (see Fig. 5) that can be similarly manipulated through external perturbations. The heavy 5d iridium ions in these materials provide exceptionally strong spin–orbit coupling, while the pyrochlore lattice geometry creates ideal conditions for realizing the effective $j_{\rm eff} = 1/2$ and $j_{\rm eff} = 3/2$ physics in Fig. 1. Specifically, the Luttinger semimetal in $Pr_2Ir_2O_7$ arises mostly from the $j_{\rm eff} = 1/2$ manifold instead of the $j_{\rm eff} = 3/2$ manifold of four pyrochlore sublattices. Experimental studies using angle-resolved photoemission spectroscopy have directly visualized the characteristic band degeneracies [20], while transport measurements reveal the unique electronic responses expected for the Luttinger semimetals. The theoretical description of these iridate materials employs the same mathematical framework and topological invariants developed for p-electron topological insulators and semimetals, underscoring their hidden physical equivalence. The parallel presence of similar physics in both p-orbital and t_{2g} material classes provides compelling evidence for their fundamental connection through orbital homology.

The comparative analysis across these material systems reveals universal physical signatures, including enhanced density of states near band touching points, non-Fermi liquid behaviors [21], specific heat following distinctive power laws at low temperatures, and unusual magnetotransport behavior arising from non-trivial Berry curvature distributions. Most importantly, both p-orbital and t_{2g} systems exhibit similar responses to symmetry-breaking perturbations, following parallel pathways in their transitions to descendant topological and correlated phases. This universal behavior underscores that essential physics is dictated not by specific orbital origin but by symmetry properties and algebraic structure of the effective Hamiltonian, establishing the p-t_{2g} correspondence as a powerful design principle for quantum materials exploration.

Beyond the Luttinger semimetal context, the p-t_{2g} correspondence manifests powerfully in correlated electron systems. In heavy 5d transition metal oxides, notably the iridate family [40], the orbital homology illuminates the emergence of novel magnetic and topological states. The iridium t_{2g} electrons experience competing energy scales: crystal field splitting ($\sim$2–3 eV), Coulomb interactions ($\sim$1 eV), and remarkably strong spin–orbit coupling ($\sim$0.4 eV). The spin–orbit coupling within the t_{2g} manifold, mixes orbital and spin degrees of freedom to form total angular momentum $j_{\rm eff}$ states (see Fig. 1). The t_{2g}^5 electronic configuration of Ir^{4+} ions gives rise to a $j_{\rm eff} = 1/2$ ground state, conceptually analogous to the $j = 1/2$ state that would arise from a p^1 configuration. This $j_{\rm eff} = 1/2$ state exhibits unusual properties including anisotropic exchange interactions, canted antiferromagnetism, and proposed topological characteristics, and would in principle find natural relevance in the p-orbital analogue system if the strong correlation is present.

The power of the p-t_{2g} homology extends to early transition metal oxides such as $SrTiO_3$ [41–44]. In $SrTiO_3$, the Ti t_{2g} electrons display a rich phase diagram including superconductivity at low carrier densities, unusual ferroelectric-like behavior, and possible orbital ordering. The t_{2g} manifold's response to various perturbations, including strain, electric fields, and doping, closely mirrors how a p-orbital system would behave under equivalent symmetry-breaking conditions. The multi-band superconducting behavior and its sensitivity to disorder can be understood through the multi-orbital pairing symmetry derived from the t_{2g} basis, which maps directly onto a p-orbital pairing problem. This perspective may be useful in explaining why certain scattering mechanisms strongly suppress superconductivity while others have minimal effect, based on the orbital character of the participating states.

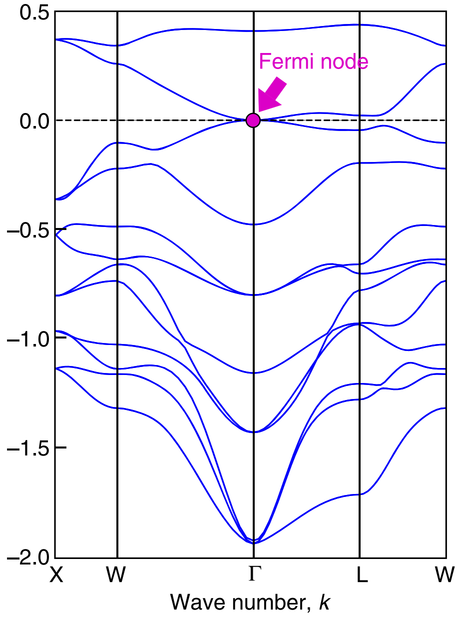

Fig. 5. The electronic band structure of $Pr_2Ir_2O_7$ from density functional theory (DFT). The Ir t_{2g} electrons, under strong spin–orbit coupling, form j_{eff} states. On the pyrochlore lattice, the four sublattices provide an internal degree of freedom that enables the formation of a quadratic band touching at the Γ point, primarily derived from the $j_{\mathrm{eff}} = 1/2$ bands. This results in a Luttinger semimetal phase, where the low-energy physics is described by an effective Luttinger-type model but originates from the $j_{\mathrm{eff}} = 1/2$ manifold coupled to the lattice symmetry. Energy unit is in eV.
Source: Figure is adapted from Ref. [20].

This unifying perspective reveals underlying connections between materials that would otherwise appear unrelated, and will stimulate cross-fertilization between research communities that traditionally focused on different material classes, accelerating progress in the understanding and design of complex quantum materials. By recognizing that t_{2g} systems can emulate the physics of p-orbital models, researchers can translate theoretical predictions from well-studied p-orbital contexts to the more complex realm of transition metal compounds, except that the t_{2g} systems can be more correlated than the p-orbital systems. The similar phenomenology observed in the p-electron systems like bismuth-based topological insulators and t_{2g}-based transition metal oxides, including their response to spin–orbit coupling, tendency toward nematic ordering, and unconventional superconducting instabilities, stems from their shared orbital properties. From the spin–orbit-driven magnetism of iridates [45] to the complex orbital physics of titanates [3] and the topological states in various 4d and 5d compounds, this orbital homology illuminates the underlying mechanisms and emergent behaviors across diverse material families. By establishing this correspondence, we not only improve our understanding of the existing materials but also gain a useful framework for predicting and engineering new quantum states in transition metal compounds, harnessing the rich interplay between orbital, spin, charge, and lattice degrees of freedom that characterizes these materials.

3. Two-dimensional materials and interfaces

The functional equivalence and homology between the p and t_{2g} orbital systems manifest with particular clarity in low-dimensional structures and selected bulk materials, where quantum confinement, symmetry breaking, and specific crystal field environments create ideal conditions for observing this profound correspondence. Among these systems, the two-dimensional electron gases (2DEGs) formed at the interfaces of perovskite oxides, including the extensively studied $LaAlO_3/SrTiO_3$ system [46–52] and the more recent $LaAlO_3/KTaO_3$ heterostructures [53–56], provide compelling platforms for exploring the deep connections between orbital physics and emergent quantum phenomena. Remarkably, this p-t_{2g} equivalence extends beyond artificial heterostructures to bulk iron-based superconductors, where the tetrahedral crystal field and potential e_g-t_{2g} level inversion in the FeX_4 (X = As, Se, Te) coordination environment enable topological band structures and even Majorana zero modes [57–61]. These diverse quantum systems collectively reveal how the complex behavior of transition metal d-electrons can be understood through the more intuitive framework of p-orbital physics, while also highlighting remarkable parallels with topological insulator-based superconductors such as Cu-doped Bi_2Se_3 [62–69], establishing orbital homology as a useful principle across different material platforms and dimensionalities.

3.1. Heterostructure interfaces

In the $LaAlO_3/SrTiO_3$ interface, the conduction electrons predominantly occupy the titanium t_{2g} orbitals. The transition from bulk three-dimensional crystal to two-dimensional confinement induces a fundamental reorganization of the orbital energy landscape. While the t_{2g} manifold remains degenerate in bulk $SrTiO_3$ under cubic crystal field symmetry, the interfacial environment breaks this degeneracy through two primary mechanisms, the structural asymmetry normal to the interface plane and the electrostatic confinement potential that localizes electrons within a narrow quantum well. This confinement selectively affects the different t_{2g} orbitals based on their spatial orientation relative to the interface. For the (001) interface, there exists a well-known interfacial electronic reconstruction that creates a two-dimensional electron gas at the interface (see Fig. 6) [46,47,70]. The d_{xy} orbital, with its electron density concentrated within the interfacial plane, experiences the strongest quantum confinement effect. In contrast, the d_{xz} and d_{yz} orbitals, characterized by their out-of-plane spatial extension, respond less dramatically to the two-dimensional confinement.

More recently, the $LaAlO_3/KTaO_3$ heterostructure has emerged as a particularly intriguing system that exhibits even stronger spin–orbit coupling effects due to the heavy tantalum element. When fabricated along the (111) crystallographic direction, this interface displays remarkable superconducting properties below approximately 2 K [53–56], with the superconducting state exhibiting clear signatures of nematic behavior [71]. The t_{2g} orbitals in this geometry arrange in a triangular lattice that naturally hosts complex orbital textures, while the strong atomic spin–orbit coupling of the $5d$ tantalum electrons, significantly enhanced compared to the $3d$ titanium electrons in $SrTiO_3$, generates substantial mixing between the orbital and spin degrees of freedom. This strong spin–orbit coupling, operating within the t_{2g} manifold with its effective $l = 1$ character, plays a crucial role in stabilizing the unconventional superconducting state observed in these interfaces.

The emergent physics of the t_{2g} orbitals in these oxide interfaces exhibits remarkable functional equivalence to the well-understood p-orbital systems. In particular, the (xz, yz) doublet of the (001) interface behaves analogously to a two-dimensional p_x-p_y system in its fundamental orbital symmetry and quasi-one-dimensional hopping characteristics, where the d_{xz} orbital demonstrates strong hopping along the x-direction but significantly weaker hopping along the perpendicular y-direction, precisely mirroring the directional dependence of a p_x orbital (see Fig. 2). Simultaneously, the d_{yz} orbital displays the complementary behavior, echoing the properties of a p_y orbital. Furthermore, from the perspective of its response to structural inversion asymmetry and the resulting Rashba effect, the system behaves similarly to a p_z-like doublet under interfacial potential gradients.

The emergence of ferromagnetism at the $LaAlO_3/SrTiO_3$ interface [50] finds a fundamental explanation through the lens of p-t_{2g} orbital homology [72,73], revealing a universal mechanism for itinerant ferromagnetism in multi-orbital systems. Within the 2DEG, the t_{2g}-derived (d_{xz}, d_{yz}) doublet behaves as an effective (p_x, p_y) orbital system. This orbital-selective hopping anisotropy creates distinct bandwidths and energy dispersions for different orbital states (see Fig. 6), a condition known to promote ferromagnetic instability in multi-orbital systems. Crucially, the presence of inter-orbital Hund's coupling provides the essential interaction that aligns electron spins across different orbital channels, while the anisotropic hopping ensures the kinetic energy gain through ferromagnetic alignment. The mechanism can be well described by the following multiple-orbital model [72,73],

$$H = H_0 + H_I, \tag{4}$$

$$\mathcal{H}_0 = \sum_{\mathbf{k},\alpha} \frac{k_x^2 + k_y^2}{2m_0} a^\dagger_{0\alpha}(\mathbf{k}) a_{0\alpha}(\mathbf{k}) + \sum_{\mathbf{k},\alpha,i=x,y} \left(\Delta + \frac{k_i^2}{2m_i} \right) a^\dagger_{i\alpha}(\mathbf{k}) a_{i\alpha}(\mathbf{k}), \tag{5}$$

$$\mathcal{H}_I = U \sum_{\mathbf{r},i} n_{i\uparrow}(\mathbf{r}) n_{i\downarrow}(\mathbf{r}) + U' \sum_{\mathbf{r},i\neq j} n_i(\mathbf{r}) n_j(\mathbf{r}), -J_H \sum_{\mathbf{r},i\neq j} \mathbf{S}_i(\mathbf{r}) \cdot \mathbf{S}_j(\mathbf{r}), \tag{6}$$

where $a_{0\alpha}, a_{x\alpha}, a_{y\alpha}$ describe the xy, xz, and yz bands (with spin polarization $\alpha = \uparrow, \downarrow$), respectively. m_0 is the effective mass for the xy orbital, m_i ($i = x, y$) is the effective mass for yz and xz orbitals, and Δ is the subband crystal field splitting. We have assumed a tetragonal crystal field symmetry for the (001) interface in Eq. (4), so $m_x = m_y$, and the one-dimensional hopping of the xz/yz orbital is assumed as the limiting regime for the Luttinger liquid description. Moreover, $n_{i\alpha}(\mathbf{r}) = a^\dagger_{i\alpha}(\mathbf{r}) a_{i\alpha}(\mathbf{r})$, $n_i(\mathbf{r}) = \sum_\alpha n_{i\alpha}(\mathbf{r})$, and $\mathbf{S}_i(\mathbf{r}) = \frac{1}{2} \sum_{\alpha\beta} a^\dagger_{i\alpha}(\mathbf{r}) \sigma_{\alpha\beta} a_{i\beta}(\mathbf{r})$. As usual, one expects the intra-orbital interaction Hubbard U to be the largest interaction, with the inter-orbital interaction U' and the Hund's coupling J_H smaller.

Within these quasi-1D bands, the electron–electron interactions are not adequately described by Fermi liquid theory. Instead, the low-energy physics is governed by the Luttinger liquid framework, where spin and charge degrees of freedom separate, and the spin fluctuations are significantly enhanced. The crucial ingredient is the Hund's coupling, J_H, which operates on the Ti sites. In this multi-orbital environment, Hund's rule favors the alignment of electron spins across the different quasi-1D channels (e.g., in the d_{xz} and d_{yz} orbitals) and the d_{xy} orbital. The enhanced spin susceptibility inherent to the Luttinger liquid state in these 1D bands amplifies this effect, providing a highly favorable environment for the ferromagnetic alignment of spins to lower the total energy via the Hund's interaction. This synergy between multi-orbital Hund's coupling and the unique correlation physics of quasi-1D Luttinger liquids offers a robust and distinct pathway to stabilize the interfacial ferromagnetic state observed in the $LaAlO_3/SrTiO_3$ interface. Even slightly away from the Luttinger

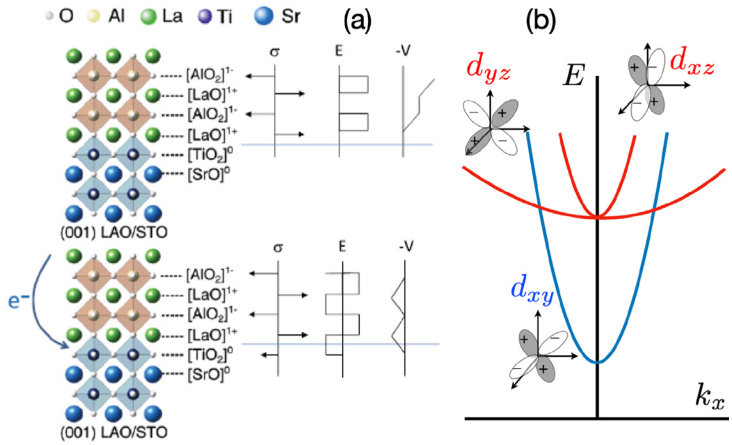

Fig. 6. (a) Electronic reconstruction process at the (001) $LaAlO_3/SrTiO_3$ interface. The polar nature of $LaAlO_3$ results in a continuously growing electrostatic potential (polar catastrophe). To stabilize the system, a charge transfer of 0.5 electrons per unit cell occurs from the surface to the interface. This transfer screens the built-in electric field, leading to a stable potential profile and the formation of a conducting two-dimensional electron gas at the interface. σ is the planer electron density, E is the surface electric field, and $-V$ is the electric potential. Figure is adapted from Ref. [70]. (b) The dispersion of the t_{2g} orbitals at the interface.

liquid limit, the argument for the ferromagnetism is expected to be valid. This mechanism finds rigorous mathematical foundation in the exact solutions of the isomorphic p-orbital models on similar lattice geometries (see Section 4) [73]. This combined effect of orbital anisotropy and Hund's coupling, operating within the framework of p-t_{2g} homology, thus establishes a universal paradigm for understanding ferromagnetic states across diverse material platforms, from oxide interfaces to engineered p-orbital systems.

Another striking parallel emerges when comparing the superconducting properties of these t_{2g}-based oxide interfaces with those of Cu-doped Bi_2Se_3, a p-orbital topological insulator that becomes superconducting upon copper intercalation [65,71,74–76]. Both systems exhibit nematic superconductivity, characterized by the spontaneous breaking of rotational symmetry in the superconducting state. In Cu-doped Bi_2Se_3, the strong spin–orbit coupling inherent to the p-orbital-derived bands of the bismuth selenide matrix stabilizes an odd-parity pairing state that transforms non-trivially under crystal rotations. Similarly, in the $LaAlO_3/KTaO_3$ (111) interface, the t_{2g} electrons, subjected to strong spin–orbit coupling and confined in a triangular lattice geometry, develop a superconducting order parameter that breaks the threefold rotational symmetry of the underlying crystal structure. This remarkable similarity between systems based on fundamentally different orbital types, p orbitals in Cu-doped Bi_2Se_3 and t_{2g} orbitals in $KTaO_3$ interfaces, highlights the universal role of spin–orbit coupling in driving nematic superconductivity, regardless of the specific orbital origin of the conducting states. This connection is especially clear once the superconducting properties are understood from the perspective of the more universal and generic Ginzburg–Landau theory.

The broader implications of this understanding extend to a growing family of complex oxide interfaces and topological materials. The p-t_{2g} correspondence provides a powerful conceptual framework for interpreting experimental observations and guiding materials design across diverse quantum systems. This perspective has proven particularly valuable in explaining the evolution of electronic properties with layer thickness, gate voltage, and strain—parameters that directly modulate the quantum confinement and orbital polarization in these systems. By mapping the complex t_{2g} orbital physics onto the more intuitive language of p-orbital systems, researchers can leverage well-established theoretical tools and physical intuitions to engineer quantum phenomena in these technologically promising materials, from topological phases to unconventional superconductivity. The deep connections between seemingly disparate materials like oxide heterostructures and topological insulators, as exemplified by the parallel nematic superconductivity in $LaAlO_3/KTaO_3$ interfaces and Cu-doped Bi_2Se_3, underscore the fundamental nature of orbital–structure relationships in determining emergent quantum behavior, opening new pathways for oxide electronics and quantum information applications.

3.2. Iron-based superconductors

The exploration of topological phenomena in low-dimensional systems, particularly at interfaces and in two-dimensional materials as discussed in previous subsections, finds a remarkable parallel in the bulk and two-dimensional electronic structure of iron-based superconductors. This connection is again rooted in the fundamental orbital homology between the iron t_{2g} orbitals and p orbitals. In iron-based superconductors [58], the iron atoms reside in a tetrahedral coordination environment formed by the pnictogen or chalcogen atoms, creating a crystal field that splits the 3d orbitals into e_g and t_{2g} manifolds that are reversed from the octahedral environment. Despite this little difference, the t_{2g} orbitals still behave as active orbitals with active spin–orbit couplings (see Fig. 7). The orbital homology between p and t_{2g} orbitals

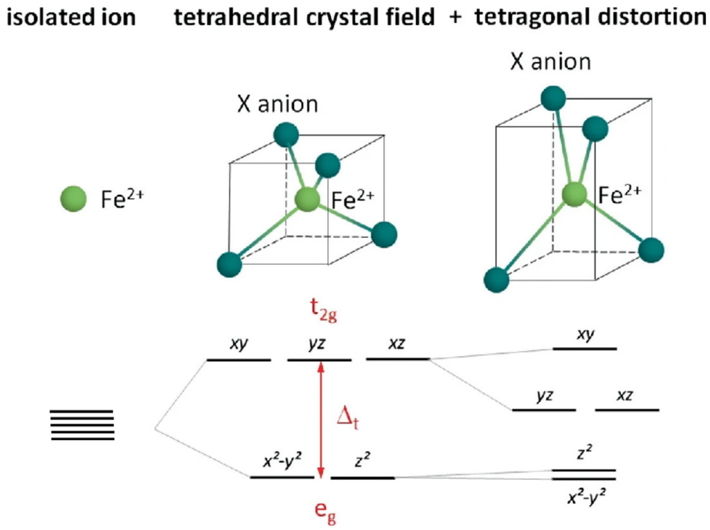

Fig. 7. Crystal field levels of the Fe 3d orbitals in Fe-based superconductors due to the tetrahedral crystal field and an additional tetragonal distortion. *Source:* Figure is adapted from Ref. [77] with modification.

manifests through two deeply connected physical phenomena, the microscopic mechanism of spin–orbit coupling driven band inversion and the subsequent emergence of topological superconductivity with Majorana zero modes. This dual demonstration reveals the p-t_{2g} equivalence as a fundamental organizing principle governing topological phenomena across disparate material classes.

The theoretical foundation of this homology lies in the similar transformation properties of the t_{2g} orbital triplet under the glide-mirror and inversion symmetries of the P4/nmm space group as the behaviors of the p orbital electrons in the relevant materials [61]. This algebraic equivalence establishes the t_{2g} manifold as an effective orbital angular momentum $l_{\mathrm{eff}} = 1$ system, directly analogous to the intrinsic $l = 1$ character of the p electrons. This mapping becomes particularly significant in materials like Fe(Te,Se) and Li(Fe,Co)As, where the combination of tetrahedral coordination, optimized anion height, and strong electron correlations creates conditions favorable for topological band inversions within the t_{2g}-derived electronic states [61].

The physical manifestations of this orbital homology are profound. The low-energy effective models describing these t_{2g}-based band inversions, whether in monolayer FeSe/$SrTiO_3$ or bulk Fe(Te,Se), are formally identical to the Bernevig–Hughes–Zhang model originally developed for p-type HgTe/CdTe quantum wells. There, strong spin–orbit coupling induces a fundamental band inversion between the s-type (Γ_6) and p-type (Γ_8) bands (see Fig. 4), with the topological nature captured by the celebrated Bernevig–Hughes–Zhang (BHZ) model [16], where the mass term changes sign at the critical thickness, signaling the topological phase transition tuned by the spin–orbit coupling. Remarkably, this identical physical picture emerges in the iron-based superconductors, albeit through the agency of t_{2g} orbitals acting as the effective p orbitals. This equivalence enables the construction of nearly identical low-energy $\mathbf{k}\cdot\mathbf{p}$ models around high-symmetry points. For instance, at the Γ point, the effective Hamiltonian takes the form [16,61],

$$H_\Gamma(\mathbf{k}) = \epsilon_0(\mathbf{k}) + \begin{bmatrix} -M(\mathbf{k}) & Ak_+ & 0 & 0 \\ Ak_- & M(\mathbf{k}) & 0 & 0 \\ 0 & 0 & -M(\mathbf{k}) & -Ak_- \\ 0 & 0 & -Ak_+ & M(\mathbf{k}) \end{bmatrix}, \tag{7}$$

where $M(\mathbf{k}) = M - B(k_x^2 + k_y^2)$, $k_\pm = k_x \pm ik_y$, precisely mirroring the BHZ form. The band inversion condition $MB > 0$, now occurring between t_{2g}-derived states of opposite parity, demonstrates conclusively that the topological band inversion mechanism transfers completely across two orbital families, and the topological transition is again driven by the spin–orbit coupling that is operates equivalently on the t_{2g} orbitals as the p orbitals. This theoretical equivalence translates directly to the parallel phenomena. The Dirac-cone surface states and helical spin textures observed in Fe(Te,Se) via ARPES represent the topological physics [58], that was first observed in the p-orbital systems, now emerging from the effective p-wave character of the t_{2g} electrons.

This orbital homology extends powerfully into the realm of topological superconductivity and Majorana physics. In conventional semiconductor-based approaches, Majorana bound states are engineered through proximity effects between s-wave superconductors and topological insulators or semiconductors with strong Rashba-type p-orbital character [78,79]. Iron-based superconductors, however, achieve this topology intrinsically through a remarkable "self-proximity effect" that leverages their multi-orbital nature [61]. The topological surface states emerging from the t_{2g}-band inversion, themselves possessing the p-orbital character, become naturally proximitized by the intrinsic $s_{\pm}$-wave bulk superconductivity of the same material. This creates an inherent platform for topological superconductivity described by an effective p-wave pairing potential, without requiring artificial heterostructures.

The experimental observations of zero-bias conductance peaks localized in the vortex cores of $FeTe_{0.55}Se_{0.45}$, exhibiting key characteristics of Majorana bound states including non-splitting behavior with spatial position and temperature scaling consistent with topological protection, provides compelling evidence that the t_{2g} electrons can emulate the complete topological pathway from band inversion to Majorana physics [58–60]. This dual demonstration, encompassing both the microscopic SOC-driven band inversion mechanism and the subsequent emergence of topological superconductivity with non-Abelian excitations, establishes the p-t_{2g} orbital homology not as a mere mathematical curiosity but as a robust physical principle capable of guiding the discovery and design of correlated topological matter across the quantum materials landscape.

4. Ultracold atoms in optical lattices as quantum simulators

The study of orbital physics in condensed matter systems faces numerous challenges, including disorder, complex interactions, and the difficulty of precisely controlling material parameters. Ultracold atoms in optical lattices provide an exceptionally clean and highly tunable alternative platform for exploring the fundamental physics of orbital systems, particularly the functional equivalence and the homology between p- and t_{2g}-orbital manifolds. These quantum atomic matter states offer unprecedented control over lattice geometry, interaction strength, and orbital degrees of freedom, enabling the simulation of complex orbital phenomena that are difficult to isolate in solid-state systems.

Optical lattices created by interfering laser beams can be engineered to produce various lattice geometries, including the cubic, hexagonal, and triangular structures. For the fermionic atoms in p-orbitals, they directly simulate p-orbital physics with remarkable fidelity. The anisotropic nature of p-orbital wavefunctions, with their directional lobes and orientation-dependent hopping amplitudes, naturally emerges in these systems. More significantly, the Hamiltonian in a cubic or square optical lattice can be precisely [73] tuned to mimic the essential physics of t_{2g} electron systems in transition metal oxides. The p_x, p_y-orbital bands in the honeycomb lattice exhibit both flat and topological band structures [80], which can also be mapped into both the t_{2g} and even e_g-orbitals in transition metal oxides [81]. This mapping is possible because both systems share the same fundamental orbital symmetry and transformation properties under the point group operations.

The key advantage of optical lattice simulations lies in their ability to isolate specific aspects of the t_{2g} physics while avoiding complications such as disorder, phonon scattering, and complex interactions that often obscure the fundamental physics in material systems. Researchers can systematically investigate phenomena such as orbital ordering, geometric frustration, and spin–orbit coupling effects by controlling experimental parameters including lattice depth, interaction strength via Feshbach resonances, and artificial gauge fields that simulate spin–orbit coupling [82]. This clean tunability makes optical lattices an ideal testbed for theoretical predictions about t_{2g} systems before attempting to observe them in solid-state materials.

4.1. Homology in flat bands

As shown in Fig. 2, one aspect of the p-t_{2g} orbital homology lies in their hopping integrals that are directly responsible for their multi-orbital band structures (including the emergence of flat bands) on different lattices. In particular, for the p_x-p_y-orbital bands in the honeycomb lattice, they are markedly different from that of graphene as shown in Fig. 8(a). There are four bands with the lower two shown in Fig. 8(a), and the dispersion of the other two are opposite to the lower ones due to the particle-hole symmetry. The bottom and top bands are flat. They can be constructed as superpositions of a set of degenerate localized eigenstates depicted in Fig. 8(b), which exists in each hexagonal plaquette as a combined effect of destructive quantum interference and hopping anisotropy. The exquisite control in a clean, tunable environment allows for the isolated study of flat-band-driven correlation physics, such as Wigner crystallization [83] or itinerant ferromagnetism [84]. The middle two bands exhibit the same dispersion as in graphene also with Dirac cones, but their wavefunctions are very different. They provide a new mechanism for large topological gap opening beyond the s-p band inversion mechanism [85]. The flat and dispersive bands exhibit quadratic touching, which can be lifted by spontaneously developing the quantum anomalous Hall state.

The formation and character of flat bands originating from the t_{2g} and p- orbitals highlight both the deep connection through orbital symmetry and a stark contrast in the material realization. In correlated oxide interfaces [86], flat bands emerge from the t_{2g} manifold as a consequence of strong quantum confinement, lattice distortion, and orbital ordering at the two-dimensional interface. These bands, often intertwined with spin–orbit coupling and intrinsic disorder, lead to massively enhanced electron correlations and are implicated in emergent phenomena like interface magnetism and possible superconductivity [87]. While t_{2g}-based flat bands offer a complex, "real-world" platform where correlations compete with other degrees of freedom, the p-orbital flat bands provide a pristine, minimalist quantum simulator to validate fundamental theories, both united by the shared role of anisotropic orbital wavefunctions in generating quenched dispersion and strong interaction effects.

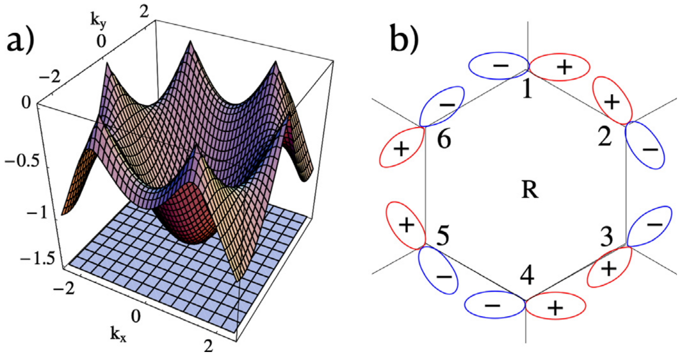

Fig. 8. (a) The energy spectra of the p_x and p_y-orbital bands, including the bottom flat-band and dispersive Dirac band. The spectra are symmetric with respect to zero, and only the lower two bands are shown. (b) The localized eigenstate for the flat band.
Source: Adapted from Ref. [80].

4.2. Itinerant ferromagnetism with p-orbitals

A particularly intriguing application of these orbital optical lattices is the study of itinerant ferromagnetism in multi-orbital systems. In condensed matter physics, the emergence of ferromagnetism in itinerant electron systems has long been a subject of intense study, with the Stoner criterion providing the basic condition for ferromagnetic instability in the single-band systems. Nevertheless, the Stoner criterion neglects correlation effects and thus overestimates the ferromagnetism tendency. In fact, even under very strong repulsions, electrons in solids often remain paramagnetic. In multi-orbital systems like those described by t_{2g} orbitals that we have discussed in Section 3, the situation becomes considerably more complex and rich. The orbital degrees of freedom introduce new channels for exchange interactions, particularly through the Hund's coupling, which favors parallel alignment of spins across different orbitals on the same atomic site.

In the p-orbital optical lattices, researchers can engineer multi-orbital systems where atoms occupy different p-orbital states (p_x, p_y, p_z) simultaneously. The anisotropic nature of orbital hopping, combined with carefully tuned interatomic interactions, creates conditions favorable for itinerant ferromagnetism through several distinct mechanisms. Isomorphic models as Eq. (4) with the form of the multi-orbital extended Hubbard model can be constructed for these p-orbital ultracold atom systems on the relevant optical lattices. Exact results of itinerant ferromagnetism on square and cubic lattices were established in the limit of infinite U, and the ferromagnetism is expected to extend to the strong coupling regime [73]. This phenomenon bears striking resemblance to the itinerant ferromagnetism observed in t_{2g} systems such as $SrRuO_3$ [88], where the complex interplay between orbital and spin degrees of freedom stabilizes the ferromagnetic state. The optical lattice platform allows researchers to systematically map out the phase diagram of this orbital-driven ferromagnetism as a function of interaction strength, filling factor, and lattice geometry, providing crucial insights into the underlying mechanisms.

4.3. Orbital homology in the Mott regime

The profound equivalence between the electronic structures of p- and t_{2g}-orbital manifolds extends beyond single-particle band topology into the deeply correlated Mott insulating regime, as exemplified by the emergence of the quantum compass model in both systems. For the p-band Mott insulators, it can be demonstrated that the spinless fermions confined to the anisotropic p_x and p_y orbitals of a two-dimensional optical lattice give rise, in the strong-coupling limit, to a highly directional superexchange interaction [89]. This interaction, derived from the stark anisotropy of the orbital-lobe-directed hopping integrals, maps onto a quantum compass model. For a bond along a general direction of $\hat{e}_\phi = \cos\phi \hat{e}_x + \sin\phi \hat{e}_y$, the exchange has a compass form as

$$H_{ex} = J_{\parallel}[\vec{\tau}(\vec{r}) \cdot \hat{e}_{2\phi}][\vec{\tau}(\vec{r} + \hat{e}_\phi) \cdot \hat{e}_{2\phi}], \tag{8}$$

where, the pseudospin vector operator $\vec{\tau} = (\tau^x, \tau^y)$ represents the two-fold orbital degrees of freedom, and the exchange anisotropy is directly frozen-in by the orbital geometry, leading to frustrated interactions and complex orbital ordering on different lattice geometries.

When applying the orbital exchange Hamiltonian Eq. (8) to the honeycomb lattice, it leads to a quantum compass model. It has a close connection to the Kitaev interaction in the Kitaev model where the exchange of each bond is essentially Ising-like and bond-dependent. It is noted that, the Kitaev interaction can be realized with the $j_{\text{eff}} = 1/2$ local moment of the t_{2g} electrons subject to strong spin–orbit coupling (see Section 2) [10,45]. Here in Eq. (8), the Ising axes can be just chosen as the bond orientation by using a set of suitable basis. The compass model is not exactly solvable, but is heavily frustrated. Its classical ground states are mapped into configurations of the fully-packed loop model with an extra $U(1)$ rotation degree of freedom. Quantum fluctuations select a six-site plaquette ground state ordering pattern in the semiclassical limit from the "*order from disorder*" mechanism.

If the residing p-orbital fermion carries the spin, the resulting model should involve the spin exchange as well, and the model is often known as Kugel–Khomskii spin–orbital exchange model in the condensed matter community. The very same effective models were known to govern the low-energy physics of certain t_{2g}-based or e_g-based transition metal oxides in their Mott insulating state for a long history [3,90,91]. This direct correspondence underscores that the p-t_{2g} homology is not merely a single-particle coincidence but a robust principle that persists into the core of strongly correlated physics. It provides a foundational justification for using the pristine, tunable p-orbital optical lattices to quantum simulate the complex orbital ordering and magnetic frustration phenomena observed in correlated t_{2g}-electron materials.

The connection to t_{2g} physics becomes particularly evident when considering the role of orbital frustration in promoting magnetic ordering. As we have remarked, in both p-orbital optical lattices and t_{2g} electron systems, the directional nature of orbital hopping can lead to strong frustration [3,89], where competing interactions prevent the system from finding a unique ground state. This frustration, combined with Hund's coupling that favors parallel spin alignment across orbitals, can drive the system toward a ferromagnetic state as one way to relieve the orbital frustration. Optical lattice experiments could explore this physics by engineering lattice geometries that enhance orbital frustration and studying the resulting magnetic correlations through quantum gas microscopy and other advanced detection techniques.

Furthermore, the optical lattice platform enables the investigation of how spin–orbit coupling influences itinerant ferromagnetism in multi-orbital systems. By introducing artificial gauge fields or laser-induced tunneling methods, researchers can engineer synthetic spin–orbit coupling that mimics the relativistic effects in t_{2g} materials. This capability is particularly valuable for understanding materials like Sr_2RuO_4 [92], where spin–orbit coupling plays a crucial role in determining the magnetic and superconducting properties. The combination of orbital degrees of freedom, tunable interactions, and synthetic spin–orbit coupling in optical lattices creates a powerful simulator for exploring the rich phase diagrams of t_{2g} systems, including the competition between magnetic, superconducting, and orbital-ordered phases.

4.4. Orbital quantum simulator

The insights gained from p-orbital optical lattice experiments have significant implications for our understanding of the t_{2g} materials. The study of orbital-driven ferromagnetism in optical lattices offers new perspectives on the long-standing problem of itinerant ferromagnetism in multi-orbital systems, suggesting that orbital degrees of freedom may play a more crucial role than previously appreciated. Other orbital-related physics, such as the orbital-selective Mott transitions [93], that has been proposed to explain the peculiar properties of certain transition metal compounds with t_{2g} orbitals, may be clearly demonstrated with the p-orbital optical lattice systems. The p-orbital optical lattices serve as useful quantum simulators for t_{2g} physics, offering unparalleled control and measurement capabilities. The study of multi-orbital phenomena in these systems not only advances our fundamental understanding of orbital physics but also provides valuable guidance for the exploration and design of novel quantum materials with tailored properties. The functional equivalence and orbital homology between p and t_{2g} orbital systems, so clearly demonstrated in these artificial quantum simulators, continues to reveal deep connections between seemingly disparate physical platforms and promises to illuminate the path toward new discoveries in correlated electron physics.

5. Conclusion: Toward a unified orbital framework for quantum materials

The recognition of the orbital homology between the p and t_{2g} orbital systems represents more than just an interesting theoretical correspondence. It heralds a useful guiding scheme in how we conceptualize, design, and discover quantum materials. This orbital homology provides one unifying language that transcends traditional boundaries between different classes of materials and opens new vistas for controlling quantum matter. This framework offers a useful recipe for deciphering the complex interplay between orbital character, topology, and correlation effects across the quantum materials landscape.

The implications of this unified perspective point toward a future where materials design follows first principles guided by the orbital symmetry and topology. One can imagine the quantum materials engineered with the atomic precision, where the p-t_{2g} equivalence and homology serve as the foundational principle for creating the heterostructures with certain topological properties, superconducting states with designed symmetry breaking, and magnetic systems with chosen frustration. The ability to translate insights between p-orbital and t_{2g} systems creates a powerful useful loop, discoveries in complex transition metal compounds can inform the design of simpler p-orbital devices, while clean measurements in the p-orbital platforms can validate theoretical predictions for the t_{2g} materials. Although t_{2g} systems are usually more correlated than some p-orbital systems and the Mott physics is often inaccessible with the p orbitals, this cross-pollination would still promise to accelerate the development of the quantum materials' research despite the potential differences between these two orbital systems that can be interesting on their own.

This orbital framework suggests several transformative research directions. First, it calls for an "orbital mapping" of quantum materials that is a comprehensive classification of electronic systems based on their orbital characteristics rather than their chemical composition alone. Such a classification would reveal hidden connections between seemingly disparate materials and predict new functional relationships. This could possibly lead to a new "quantum materials genome" project [94,95], where materials are characterized and designed according to their orbital genetic code, the specific combination of orbital symmetries, spin–orbit coupling strengths, and correlation effects that determine their quantum properties. Second, it points toward the development of "orbital engineering" as a distinct discipline, where materials are designed specifically to optimize desired orbital characteristics for particular applications, much like the bandgap engineering in the semiconductor technology. Third, it suggests new pathways for discovering unconventional superconductors, quantum spin liquids, and other exotic states by leveraging the guiding principles revealed through the orbital homology.

The experimental implications are equally profound. Advanced synthesis techniques, from molecular beam epitaxy of oxide heterostructures to optical lattice engineering with ultracold atoms, can now be guided by this unified orbital principle. The ability to create "orbital heterostructures", where materials with complementary orbital characteristics are combined to produce emergent phenomena, represents an exciting frontier. Similarly, the time-resolved spectroscopies could track the orbital dynamics across different material systems, revealing possibly universal behaviors in how orbitals respond to external perturbations and participate in phase transitions.

As we advance into this new perspective, the p-t_{2g} homology serves as both a guiding light and a call to action. It challenges us to rethink material categories, to develop new theoretical tools that embrace orbital complexity, and to create experimental platforms that exploit the orbital degrees of freedom. Most importantly, it reminds us that beneath the staggering diversity of quantum materials lies an underlying unity, a set of universal principles governed by symmetry and topology that transcend specific material implementations. By embracing this unified orbital perspective, we open the door to a future where quantum materials are not just discovered, but truly designed by atoms and by orbitals to meet the technological challenges.

Finally, it is crucial to recognize that the p-t_{2g} homology, while powerful, does not imply that the two systems are physically identical in all circumstances. The equivalence strictly concerns the local transformation properties under the octahedral point group and the resulting effective $l = 1$ algebra for the t_{2g} triplet. The spatial wavefunctions of the p and t_{2g} orbitals are actually different. The p orbitals are quasi-1D, with lobes pointing along the bond directions, whereas the t_{2g} orbitals have a more 2D character, with lobes lying in the planes perpendicular to the bonding axes. Consequently, the intersite hopping integrals, and hence the tight-binding band structures and exchange interactions depend sensitively on lattice geometry and the nature of chemical bonding. Therefore, while the p-t_{2g} homology provides a valuable unifying framework and a powerful design principle, its application to real materials must always be accompanied by an analysis of the specific lattice structure, orbital geometry, and hopping topology. Recognizing both the unity and the distinctions is essential for a balanced understanding and for avoiding the unexpected oversimplifications.

CRediT authorship contribution statement

Gang v. Chen: Writing – review & editing, Writing – original draft, Visualization, Methodology, Investigation, Funding acquisition, Formal analysis, Conceptualization. **Congjun Wu:** Writing – original draft, Conceptualization.

Declaration of competing interest

The authors declare that they have no known competing financial interests or personal relationships that could have appeared to influence the work reported in this paper.

Acknowledgments

We thank G. Khaliullin and Mike Norman for suggestion. GC is supported by NSFC No. 92565110, No. 12574061, and BJNSF, China with No. F261004. CW is supported by the National Natural Science Foundation of China under the Grant No. 12234016 and the New Cornerstone Science Foundation, China.

References

[1] P.W. Anderson, Basic notions of condensed matter physics, in: Frontiers in Physics, vol. 55, Benjamin-Cummings Publishing Company, Menlo Park, California, 1984, ISBN: 978-0805331620.
[2] P.W. Anderson, Concepts in Solids: Lectures on the Theory of Solids, World Scientific, Singapore, 1997, ISBN: 978-9810236312, originally published by Benjamin in 1963.
[3] S. Maekawa, S.E. Barnes, et al., Physics of transition metal oxides, in: Springer Series in Solid-State Sciences, vol. 144, Springer, Berlin, ISBN: 3540212930, 2004.
[4] D.I. Khomskii, Transition metal compounds, Cambridge University Press, Cambridge, ISBN: 978-1-107-02017-7, 2014, hardback.
[5] J.H. Van Vleck, Phys. Rev. 41 (1932) 208.
[6] M.H.L. Pryce, Phys. Rev. 80 (1950) 1107.
[7] J.S. Griffith, The Theory of Transition-Metal Ions, Cambridge University Press, Cambridge, England, 1961.
[8] A. Abragam, B. Bleaney, Electron Paramagnetic Resonance of Transition Ions, Clarendon Press, Oxford, 1970.
[9] G. Cao, J. Bolivar, S. McCall, J.E. Crow, R.P. Guertin, Phys. Rev. B 57 (1998) R11039, https://link.aps.org/doi/10.1103/PhysRevB.57.R11039.
[10] G. Jackeli, G. Khaliullin, Phys. Rev. Lett. 102 (2009) 017205, https://link.aps.org/doi/10.1103/PhysRevLett.102.017205.
[11] G. Chen, L. Balents, Phys. Rev. B 78 (2008) 094403, https://link.aps.org/doi/10.1103/PhysRevB.78.094403.
[12] H. Katsura, N. Nagaosa, A.V. Balatsky, Phys. Rev. Lett. 95 (2005) 057205, https://link.aps.org/doi/10.1103/PhysRevLett.95.057205.

[13] B.Q. Lv, T. Qian, H. Ding, Rev. Modern Phys. 93 (2021) 025002, https://link.aps.org/doi/10.1103/RevModPhys.93.025002.
[14] H. Gao, J.W. Venderbos, Y. Kim, A.M. Rappe, Annu. Rev. Mater. Res. 49 (2019) 153, http://dx.doi.org/10.1146/annurev-matsci-070218-010049.
[15] J.M. Luttinger, Phys. Rev. 102 (1956) 1030, https://link.aps.org/doi/10.1103/PhysRev.102.1030.
[16] B.A. Bernevig, T.L. Hughes, S.-C. Zhang, Science 314 (2006) 1757–1761, http://dx.doi.org/10.1126/science.1133734.
[17] D. Zhang, H. Wang, J. Ruan, G. Yao, H. Zhang, Phys. Rev. B 97 (2018a) 195139, https://link.aps.org/doi/10.1103/PhysRevB.97.195139.
[18] X. Dai, T.L. Hughes, X.-L. Qi, Z. Fang, S.-C. Zhang, Phys. Rev. B 77 (2008) 125319, https://link.aps.org/doi/10.1103/PhysRevB.77.125319.
[19] S. Murakami, N. Nagaosa, S.-C. Zhang, Phys. Rev. B 69 (2004) 235206, https://link.aps.org/doi/10.1103/PhysRevB.69.235206.
[20] T. Kondo, M. Nakayama, R. Chen, J.J. Ishikawa, E.-G. Moon, T. Yamamoto, Y. Ota, W. Malaeb, H. Kanai, Y. Nakashima, et al., Nat. Commun. (ISSN: 2041-1723) 6 (2015) http://dx.doi.org/10.1038/ncomms10042.
[21] E.-G. Moon, C. Xu, Y.B. Kim, L. Balents, Phys. Rev. Lett. 111 (2013) 206401, https://link.aps.org/doi/10.1103/PhysRevLett.111.206401.
[22] X.-P. Yao, G. Chen, Phys. Rev. X 8 (2018) 041039, https://link.aps.org/doi/10.1103/PhysRevX.8.041039.
[23] P. Zhu, R.-X. Zhang, Phys. Rev. B 110 (2024) 165120, https://link.aps.org/doi/10.1103/PhysRevB.110.165120.
[24] A.L. Szabó, R. Moessner, B. Roy, Phys. Rev. B 103 (2021) 165139, https://link.aps.org/doi/10.1103/PhysRevB.103.165139.
[25] L. Fu, Phys. Rev. Lett. 115 (2015) 026401, https://link.aps.org/doi/10.1103/PhysRevLett.115.026401.
[26] S. Hayami, Y. Yanagi, H. Kusunose, Y. Motome, Phys. Rev. Lett. 122 (2019) 147602, https://link.aps.org/doi/10.1103/PhysRevLett.122.147602.
[27] J.W. Harter, Z.Y. Zhao, J.-Q. Yan, D.G. Mandrus, D. Hsieh, Science (ISSN: 1095-9203) 356 (2017) 295–299, http://dx.doi.org/10.1126/science.aad1188.
[28] C.L. Kane, E.J. Mele, Phys. Rev. Lett. 95 (2005a) 226801, https://link.aps.org/doi/10.1103/PhysRevLett.95.226801.
[29] C.L. Kane, E.J. Mele, Phys. Rev. Lett. 95 (2005b) 146802, https://link.aps.org/doi/10.1103/PhysRevLett.95.146802.
[30] A. Shitade, H. Katsura, J. Kuneš, X.-L. Qi, S.-C. Zhang, N. Nagaosa, Phys. Rev. Lett. 102 (2009) 256403, https://link.aps.org/doi/10.1103/PhysRevLett.102.256403.
[31] L. Du, T. Li, W. Lou, X. Wu, X. Liu, Z. Han, C. Zhang, G. Sullivan, A. Ikhlassi, K. Chang, et al., Phys. Rev. Lett. 119 (2017) 056803, https://link.aps.org/doi/10.1103/PhysRevLett.119.056803.
[32] B.M. Ferrari, F. Marcantonio, F. Murphy-Armando, M. Virgilio, F. Pezzoli, Phys. Rev. Res. 5 (2023) L022035, https://link.aps.org/doi/10.1103/PhysRevResearch.5.L022035.
[33] M. Meyer, J. Baumbach, S. Krishtopenko, A. Wolf, M. Emmerling, S. Schmid, M. Kamp, B. Jouault, J.-B. Rodriguez, E. Tournie, et al., Sci. Adv. 11 (2025) eadz2408, http://dx.doi.org/10.1126/sciadv.adz2408.
[34] T.S. Ghiasi, D. Petrosyan, J. Ingla-Aynés, T. Bras, K. Watanabe, T. Taniguchi, S. Mañas-Valero, E. Coronado, K. Zollner, J. Fabian, et al., Nat. Commun. 16 (2025) 5336, http://dx.doi.org/10.1038/s41467-025-60377-1.
[35] J. c. v. Chaloupka, G. Jackeli, G. Khaliullin, Phys. Rev. Lett. 105 (2010) 027204, https://link.aps.org/doi/10.1103/PhysRevLett.105.027204.
[36] A. Bouhon, A.M. Black-Schaffer, R.-J. Slager, Phys. Rev. B 100 (2019) 195135, https://link.aps.org/doi/10.1103/PhysRevB.100.195135.
[37] A. Alexandradinata, X. Dai, B.A. Bernevig, Phys. Rev. B 89 (2014) 155114, https://link.aps.org/doi/10.1103/PhysRevB.89.155114.
[38] Y. Hwang, J. Ahn, B.-J. Yang, Phys. Rev. B 100 (2019) 205126, https://link.aps.org/doi/10.1103/PhysRevB.100.205126.
[39] Y. Nakajima, R. Hu, K. Kirshenbaum, A. Hughes, P. Syers, X. Wang, K. Wang, R. Wang, S.R. Saha, D. Pratt, et al., Sci. Adv. 1 (2015) e1500242, http://dx.doi.org/10.1126/sciadv.1500242.
[40] W. Witczak-Krempa, G. Chen, Y.B. Kim, L. Balents, Annu. Rev. Condens. Matter Phys. 5 (2014) 57, http://dx.doi.org/10.1146/annurev-conmatphys-020911-125138.
[41] M.N. Gastiasoro, J. Ruhman, R.M. Fernandes, Ann. Physics (ISSN: 0003-4916) 417 (2020) 168107, http://dx.doi.org/10.1016/j.aop.2020.168107.
[42] J.F. Schooley, W.R. Hosler, M.L. Cohen, Phys. Rev. Lett. 12 (1964) 474, https://link.aps.org/doi/10.1103/PhysRevLett.12.474.
[43] S. Salmani-Rezaie, K. Ahadi, W.M. Strickland, S. Stemmer, Phys. Rev. Lett. 125 (2020) 087601, https://link.aps.org/doi/10.1103/PhysRevLett.125.087601.
[44] T.F. Nova, A.S. Disa, M. Fechner, A. Cavalleri, Science (ISSN: 1095-9203) 364 (2019) 1075–1079, http://dx.doi.org/10.1126/science.aaw4911.
[45] G. Cao, L. DeLong, Physics of Spin-Orbit-Coupled Oxides, Oxford University Press, USA, Oxford, ISBN: 978-0-19-960202-5, 2021.
[46] A. Ohtomo, H.Y. Hwang, Nature 427 (2004) 423.
[47] H.Y. Hwang, Y. Iwasa, M. Kawasaki, B. Keimer, N. Nagaosa, Y. Tokura, Nat. Mater. 11 (2012) 103.
[48] S. Thiel, G. Hammerl, A. Schmehl, C.W. Schneider, J. Mannhart, Science 313 (2006) 1942.
[49] C. Cen, S. Thiel, G. Hammerl, C.W. Schneider, K.E. Andersen, C.S. Hellberg, J. Mannhart, J. Levy, Nat. Mater. 7 (2008) 298.
[50] J.A. Bert, B. Kalisky, C. Bell, M. Kim, Y. Hikita, H.Y. Hwang, K.A. Moler, Nat. Phys. 7 (2011) 767.
[51] N. Reyren, S. Thiel, A.D. Caviglia, L.F. Kourkoutis, G. Hammerl, C. Richter, C.W. Schneider, T. Kopp, A.-S. Rüetschi, D. Jaccard, et al., Science 317 (2007) 1196.
[52] S. Chen, Y. Ning, C.S. Tang, L. Dai, S. Zeng, K. Han, J. Zhou, M. Yang, Y. Guo, C. Cai, et al., Adv. Electron. Mater. 10 (2024) 2300730, https://advanced.onlinelibrary.wiley.com/doi/abs/10.1002/aelm.202300730.
[53] X.B. Cheng, M. Zhang, Y.Q. Sun, G.F. Chen, M. Qin, T.S. Ren, X.S. Cao, Y.W. Xie, J. Wu, Phys. Rev. X 15 (2025) 021018, https://link.aps.org/doi/10.1103/PhysRevX.15.021018.
[54] Z. Chen, Y. Liu, H. Zhang, Z. Liu, H. Tian, Y. Sun, M. Zhang, Y. Zhou, J. Sun, Y. Xie, Science (ISSN: 1095-9203) 372 (2021) 721–724, http://dx.doi.org/10.1126/science.abb3848.
[55] H. Zhang, H. Zhang, X. Yan, X. Zhang, Q. Zhang, J. Zhang, F. Han, L. Gu, B. Liu, Y. Chen, et al., ACS Appl. Mater. & Interfaces 9 (2017) 36456, http://dx.doi.org/10.1021/acsami.7b12814.
[56] C. Liu, X. Zhou, D. Hong, B. Fisher, H. Zheng, J. Pearson, J.S. Jiang, D. Jin, M.R. Norman, A. Bhattacharya, Nat. Commun. 14 (2023) 951, http://dx.doi.org/10.1038/s41467-023-36309-2.
[57] G. Xu, B. Lian, P. Tang, X.-L. Qi, S.-C. Zhang, Phys. Rev. Lett. (ISSN: 1079-7114) 117 (2016) http://dx.doi.org/10.1103/PhysRevLett.117.047001.
[58] P. Zhang, Z. Wang, X. Wu, K. Yaji, Y. Ishida, Y. Kohama, G. Dai, Y. Sun, C. Bareille, K. Kuroda, et al., Nat. Phys. 15 (2018b) 41–47, http://dx.doi.org/10.1038/s41567-018-0280-z.
[59] D. Wang, L. Kong, P. Fan, H. Chen, S. Zhu, W. Liu, L. Cao, Y. Sun, S. Du, J. Schneeloch, et al., Science 362 (2018) 333–335, http://dx.doi.org/10.1126/science.aao1797.
[60] P. Zhang, K. Yaji, T. Hashimoto, Y. Ota, T. Kondo, K. Okazaki, Z. Wang, J. Wen, G.D. Gu, H. Ding, et al., Science 360 (2018c) 182–186, http://dx.doi.org/10.1126/science.aan4596.
[61] N. Hao, J. Hu, Natl. Sci. Rev. 6 (2018) 213–226, http://dx.doi.org/10.1093/nsr/nwy142.
[62] Y.S. Hor, A.J. Williams, J.G. Checkelsky, P. Roushan, J. Seo, Q. Xu, H.W. Zandbergen, A. Yazdani, N.P. Ong, R.J. Cava, Phys. Rev. Lett. 104 (2010) 057001, https://link.aps.org/doi/10.1103/PhysRevLett.104.057001.
[63] S. Sasaki, M. Kriener, K. Segawa, K. Yada, Y. Tanaka, M. Sato, Y. Ando, Phys. Rev. Lett. 107 (2011) 217001, https://link.aps.org/doi/10.1103/PhysRevLett.107.217001.
[64] L. Fu, E. Berg, Phys. Rev. Lett. 105 (2010) 097001, https://link.aps.org/doi/10.1103/PhysRevLett.105.097001.
[65] S. Yonezawa, K. Tajiri, S. Nakata, Y. Nagai, Z. Wang, K. Segawa, Y. Ando, Y. Maeno, Nat. Phys. 13 (2016) 123–126, http://dx.doi.org/10.1038/nphys3907.

[66] T.H. Hsieh, L. Fu, Phys. Rev. Lett. 108 (2012) 107005, https://link.aps.org/doi/10.1103/PhysRevLett.108.107005.
[67] P. Hosur, P. Ghaemi, R.S.K. Mong, A. Vishwanath, Phys. Rev. Lett. 107 (2011) 097001, https://link.aps.org/doi/10.1103/PhysRevLett.107.097001.
[68] T.V. Bay, T. Naka, Y.K. Huang, H. Luigjes, M.S. Golden, A. de Visser, Phys. Rev. Lett. 108 (2012) 057001, https://link.aps.org/doi/10.1103/PhysRevLett.108.057001.
[69] L. Fu, Phys. Rev. B 90 (2014) 100509, https://link.aps.org/doi/10.1103/PhysRevB.90.100509.
[70] A. Rubano, M. Scigaj, F. Sánchez, G. Herranz, D. Paparo, J. Phys.: Condens. Matter. 32 (2019) 135001, http://dx.doi.org/10.1088/1361-648X/ab5ccc.
[71] G. Zhang, L. Wang, J. Wang, G. Li, G. Huang, G. Yang, H. Xue, Z. Ning, Y. Wu, J.-P. Xu, et al., Nat. Commun. (ISSN: 2041-1723) 14 (2023) http://dx.doi.org/10.1038/s41467-023-38759-0.
[72] G. Chen, L. Balents, Phys. Rev. Lett. 110 (2013) 206401, https://link.aps.org/doi/10.1103/PhysRevLett.110.206401.
[73] Y. Li, E.H. Lieb, C. Wu, Phys. Rev. Lett. 112 (2014) 217201, https://link.aps.org/doi/10.1103/PhysRevLett.112.217201.
[74] S. Davis, Z. Huang, K. Han, Ariando, T. Venkatesan, V. Chandrasekhar, Phys. Rev. B 97 (2018) 041408, https://link.aps.org/doi/10.1103/PhysRevB.97.041408.
[75] M. Hecker, J. Schmalian, Npj Quantum Mater. 3 (2018) 26, http://dx.doi.org/10.1038/s41535-018-0098-z.
[76] K. Matano, M. Kriener, K. Segawa, Y. Ando, G. q. Zheng, Nat. Phys. (ISSN: 1745-2481) 12 (2016) 852–854, http://dx.doi.org/10.1038/nphys3781.
[77] S. Haindl, Introduction to Fe-Based Superconductors, Springer International Publishing, Cham, ISBN: 978-3-030-75132-6, 2021, pp. 1–25, http://dx.doi.org/10.1007/978-3-030-75132-6_1.
[78] L. Fu, C.L. Kane, Phys. Rev. Lett. 100 (2008) 096407, https://link.aps.org/doi/10.1103/PhysRevLett.100.096407.
[79] R.M. Lutchyn, J.D. Sau, S. Das Sarma, Phys. Rev. Lett. 105 (2010) 077001, https://link.aps.org/doi/10.1103/PhysRevLett.105.077001.
[80] C. Wu, D. Bergman, L. Balents, S. Das Sarma, Phys. Rev. Lett. (ISSN: 1079-7114) 99 (2007) http://dx.doi.org/10.1103/PhysRevLett.99.070401.
[81] S. Xu, C. Wu, Quantum Front. 1 (2022) 24, http://dx.doi.org/10.1007/s44214-022-00025-7.
[82] Y. Han, Y. Wei, W. Zhang, Physics on Ultracold Quantum Gases, in: Peking University-World Scientific Advanced Physics Series, World Scientific Publishing Co., ISBN: 978-9813270756, 2019, derived from graduate courses, covers basics (laser cooling, atom-light interaction) to quantum simulation in optical lattices, ideal for researchers and graduate students, https://www.amazon.com/Physics-Ultracold-University-World-Scientific-Advanced/dp/9813270756.
[83] C. Wu, S. Das Sarma, Phys. Rev. B 77 (2008) 235107.
[84] S. Zhang, H. h. Hung, C. Wu, Phys. Rev. A 82 (2010) 053618, http://link.aps.org/doi/10.1103/PhysRevA.82.053618.
[85] G.-F. Zhang, Y. Li, C. Wu, Phys. Rev. B 90 (2014) 075114, http://link.aps.org/doi/10.1103/PhysRevB.90.075114.
[86] F. Wang, Y. Ran, Phys. Rev. B (ISSN: 1550-235X) 84 (2011) http://dx.doi.org/10.1103/PhysRevB.84.241103.
[87] M. Karmakar, Correlated electrons in flat bands: Concepts and developments, 2025, 2508.07430, https://arxiv.org/abs/2508.07430.
[88] G. Koster, L. Klein, W. Siemons, G. Rijnders, J.S. Dodge, C.-B. Eom, D.H.A. Blank, M.R. Beasley, Rev. Modern Phys. 84 (2012) 253, https://link.aps.org/doi/10.1103/RevModPhys.84.253.
[89] C. Wu, Phys. Rev. Lett. 100 (2008) 200406, https://link.aps.org/doi/10.1103/PhysRevLett.100.200406.
[90] K.I. Kugel, D.I. Khomskii, Sov. Phys. Uspekhi 25 (1982) 231, http://dx.doi.org/10.1070/PU1982v025n04ABEH004537.
[91] G. Khaliullin, Progr. Theoret. Phys. Suppl. (ISSN: 0375-9687) 160 (2005) 155, http://dx.doi.org/10.1143/PTPS.160.155.
[92] M.W. Haverkort, I.S. Elfimov, L.H. Tjeng, G.A. Sawatzky, A. Damascelli, Phys. Rev. Lett. 101 (2008) 026406, https://link.aps.org/doi/10.1103/PhysRevLett.101.026406.
[93] A. Koga, N. Kawakami, T.M. Rice, M. Sigrist, Phys. Rev. Lett. 92 (2004) 216402, https://link.aps.org/doi/10.1103/PhysRevLett.92.216402.
[94] A. Bhattacharya, I. Timokhin, R. Chatterjee, Q. Yang, A. Mishchenko, Npj Comput. Mater. 9 (2023) 101, http://dx.doi.org/10.1038/s41524-023-01056-x.
[95] D. Pablo, J. Jackson, N. Webb, M., et al., Npj Comput. Mater 5 (2019) 41.